Fuel 379 (2025) 133015

Contents lists available at ScienceDirect

Fuel

journal homepage: www.elsevier.com/locate/fuel

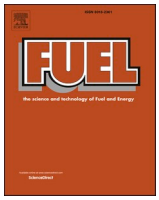

Full Length Article

Laminated shale oil system mobility and controlling factors of the Paleogene Shahejie Formation: Evidences from T_1-T_2 NMR experiments, multi-temperature pyrolysis and confocal laser scanning microscopy

Biao Sun [a,b,c], Xiaoping Liu [a,b,*], Xianzheng Zhao [a,b,d], Murray Gingras [c], Fengming Jin [e], Tian Liu [a,b], Zuxian Hua [a,b], Wendi Peng [a,b], Yu Yuan [a,b]

[a] State Key Laboratory of Petroleum Resources and Engineering, China University of Petroleum (Beijing), Beijing 102249, China
[b] College of Geosciences, China University of Petroleum (Beijing), Beijing 102249, China
[c] Department of Earth and Atmospheric Sciences, University of Alberta, Edmonton, AB T6G 2E3, Canada
[d] China Petroleum Consulting Center, Beijing 100724, China
[e] Dagang Oil Field Company of PetroChina, Tianjin 300280, China

ARTICLE INFO

Keywords:
Laminated shale
Shale oil mobility
Controlling factors
NMR T_1-T_2 map
Confocal laser scanning microscopy

ABSTRACT

Characterizing the mobility of shale oil is crucial when attempting to understand petroleum accumulation, oil recovery enhancements, as well as petroleum resources assessments for the unconventional reservoirs. That study especially in the lacustrine environment remain, however, limited and are least understood due to laminae development heterogeneity. A total of 12 core samples from the third member of the Shahejie Formation of the Bohai Bay Basin were employed to study the shale oil mobility occurred in the lacustrine strata through nuclear magnetic resonance (NMR), Rock-eval pyrolysis, and multi-temperature pyrolysis experiments. Laminas consist of bright laminae that contain high contents of quartz, feldspar, calcite, and dolomite, which are frequently intercalated with dark laminae dominated by clay and organic matter. The movable oil contents estimated by NMR (3.96–7.05 mg/g) is higher than that defined by both Rock-eval pyrolysis (0.57–3.29 mg/g Rock) and multi-temperature pyrolysis methods (0.36–5.89 mg/g Rock). This divergence is likely due to the volatility of light hydrocarbons, resulting in the NMR estimations being considered the most reliable. The movable oil content that exists within bright laminae are typically higher than that to which resides within dark laminae due to the oils generated in dark beds migrating from the dark laminae segments to bright beds. This in turn leads to the increase of the heavy components, asphaltenes, in the kerogen of the dark laminae and that of light components in the bright laminae. Combination with the reservoirs characterizations results, it suggests that the pore sizes and structures may play a critical role in the aforementioned differences in movable oil content between dark and bright beds, where bright laminae is characterized by type H2 with the diameters of 100–500 nm, while dark laminae belong to type H3 with a smaller diameter of 20–200 nm. As a result, higher levels of movable oil were trapped within inorganic pores with a diameter of 100–500 nm in bright laminae, while heavier compositions with the characteristic of low mobility were absorbed in the kerogen. These findings have a significant impact on existing knowledge around the mechanisms of shale oil enrichment and the exploitation of sweet spots.

1. Introduction

With the decrease in consumption and reserves of conventional resources and the continuous increase in energy demand, unconventional resources including shale oil have become the main exploration target [1,2]. Shale oil resources, with global technically recoverable reserves of 1.4×10^{12} t, which amounts to roughly three times the total conventional oil resources [3,4]. However, it is estimated that the total amount of successful oil recovery in oil-bearing shale reservoirs is less than 10 % [5]. Various engineering factors and the issue of limited geological data restrict our understanding of certain parameters around estimated oil recovery. It is believed that the composition of shale oil and oil saturation act as key factors that influence the evaluation of resource potential within oil reserves [6–9]. Movable oil contents are

* Corresponding author at: State Key Laboratory of Petroleum Resources and Engineering, China University of Petroleum (Beijing), Beijing 102249, China.
E-mail address: liuxiaoping@cup.edu.cn (X. Liu).

https://doi.org/10.1016/j.fuel.2024.133015
Received 13 March 2024; Received in revised form 20 July 2024; Accepted 30 August 2024
Available online 5 September 2024

also a significant component of identifying and evaluating sweet spots, primarily because movable oil tends to flow more predominately within laminae [10]. Therefore, movable oil contents in shale and controlling factors such as those mentioned above are vital in attempting to better understand the intricacies of shale oil exploitation.

The characterization of shale oil content is actually aimed at evaluating the moveable oil content. Generally, the main methods include observation [11,12], experimental analysis [13–19], and molecular dynamics simulation [20–22]. The more direct method of observation mainly employs high-resolution CT scanning, confocal laser scanning microscopy [12], and an Environmental Scanning Electron Microscope to observe the states in which shale oil exists and develops through. However, the disadvantage associated with the direct characterization method is its inability to quantitatively describe changes in the composition of movable oil at different pore sizes.

In comparison, the experimental analysis method mainly relies on geochemical parameter characterization, nuclear magnetic resonance (NMR) T_1-T_2 spectra [18], three-dimensional fluorescence experiments, rock–eval pyrolysis, and multi-temperature pyrolysis experiments [14,17], and solvent extraction experiments [16] to quantitatively evaluate the movable oil. These methods are primarily used to estimate the quantity of free hydrocarbons within the shale oil, however, limitations to these methods still make it difficult to acquire an accurate assessment of mobile hydrocarbons. The process of sample storage and the utilization of experiment equipment can also result in a reduction in both the volatility of the oil movement and the level of movable oil itself.

Due to the complex occurrence of the states in which shale oil can exist, using a single experimental method makes it difficult to accurately and quantitatively identify the characteristics of movable oil, resulting in an incomplete representation of movable oil. The current technological level that is are able to be achieved leaves much to be desired in this regard. At present, no microscopic method can effectively quantitatively evaluate the characteristics that determine movable oil within shale oil reservoirs. Attempts have been made to use molecular dynamics simulation methods to study the characteristics of movable oil and the various occurrence states of shale oil from micro to nanoscale calculations, which can also help reveal further details around shale oil enrichment mechanisms [20,21], but it is difficult to clarify the behavior of movable shale oil in complex pore systems.

Many factors have been determined to affect movable oil contents, with many scholars in previous studies focusing on aspects such as hydrocarbon generation properties [23–25], lithofacies types [26–28], reservoir storage capacity [29–33], and the fluid level [34–36]. Generally, the type of lithofacies has a great influence on shale oil mobility, with the movable oil also being affected by divergences in the wettability of different lithofacies. Laminated shale also possesses a higher proportion of movable oil than massive shale facies due to its absorption capacity and surface. It has also been identified that the pore structure of shale reservoirs can affect oil mobility due to different shale porosity and pore-throat volume distribution which can lead to differences in the occurrence characteristics of mobile fluids. Previous research has further concluded that hydrocarbon generation, especially when considering the properties of maturity (extensive hydrocarbon generation), is closely related to the movable oil content in shale [37–39]. Essentially, the greater the progression toward maturity, the greater the level of mobility will be experienced during oil generation. There are significant differences in the adsorption behaviors of different fluid components in shale oil. Generally speaking, heavy hydrocarbons tend to have stronger adsorption capacity than lighter components due to their larger molecular weight, and aromatic hydrocarbons also tend to have special chemical bonds that allow for a stronger adsorption capacity. Comparatively, non-polar components such as saturates in shale oil have weak adsorption capacity and low viscosity, which is why such components can more effectively migrate in pores. This also results in a greater chance of them being present in inorganic pores, thus creating the observed movable state. Certain components of shale oil, however, such as resins and asphaltenes with large molecular weight and a strong polarity struggle to migrate and are easily retained within pore networks formed by the kerogen, leading to these components generally presenting in an adsorbed state. Interestingly, the majority of shale movable oil within oil wells is from laminated shale [40–42]. In other words, the laminae are key to the mobility of shale oil, as they affect reservoir storage capacity and interlayered fracture development, which greatly increases the horizontal permeability [42–45]. Additionally, the deposition of organic matter and inorganic mineral matter provides favorable conditions for the generation and expulsion of hydrocarbons [46–48].

At present, researchers have discovered that laminae are closely related to the level of mobility in shale oil [49–51]. However, the quantitative characterization of movable oil content remains difficult to evaluate when only employing a single technical analytical method. Additionally, scholars have tended to focus on the characteristics of pore microstructures instead of shale oil mobility [52,53]. As a result, few investigations have explored the occurrence states of movable oil, the composition of movable oil, and the various controlling factors, which all significantly restrict the degree of movability and the production of shale oil.

Therefore, this study aims to quantitatively evaluate shale oil, specifically focusing on the movable oil content, distribution characteristics, and controlling factors of laminated shale reservoirs using the tools and methods of X-ray diffraction (XRD), total organic carbon (TOC), low-temperature nitrogen adsorption, thin section analysis, T_1-T_2 NMR, Rock–Eval pyrolysis, multi-temperature pyrolysis, and confocal laser scanning microscopy. This study primarily relied on samples of laminated shale from the Paleogene Shahejie Formation in the Bohai Bay Basin, East China, to characterize the occurrence state of movable oil, its contents, and relevant controlling factors. The results achieved were able to improve our understanding around the level of mobility in organic-rich laminated shale, which is significant to the future exploration of shale oil and the field's broader development.

2. Materials and methods

2.1. Sample Collection

The Bohai Bay Basin in East China is Approximately 200,000 km^2 in size and is divided into six depressions (Fig. 1**b**), it is commonly characterized as a large Cenozoic basin (Fig. 1**a**) [54,55]. The Huanghua depression is situated in the central region of the Bohai Bay Basin and is subsequently divided into five sags, including Banqiao, Qikou, Cangdong, Nanpi, and Yanshan (Fig. 1**c**) [56]. The Qikou Sag was the primary area explored in the Bohai Bay Basin. The basin rocks are predominantly Cenozoic, comprised of the Paleogene Kongdian (Ek), Shahejie (Es), and Dongying (Ed) formations in ascending order [57–59]. From these 3 formations, the Shahejie Formation was the primary source of sample rocks and the focal area for shale oil exploration. Said formation is split into three sub-units or members: the Es_1, Es_2, and Es_3. These members facilitated the development of the braided river delta facies, fan delta facies, offshore submerged fan facies, turbidite fan facies, and lake facies [60,61]. A total of 12 samples were collected from the Es_3 interval of Well Q1 illustrated in Fig. 1**d**. The core lithology predominantly consists of shale, spanning a depth of 3988.64 to 4077.56 m.

2.2. Methods

2.2.1. X-ray diffraction, thin section analysis, and scanning electron microscopy (SEM)

For the purpose of this study, collected samples were ground into a powder using an agate mortar for the completion of the X-ray diffraction (XRD) test. The powder was subsequently fed through the instruments, allowing for diffractograms to be analyzed by a computer using quantitative calculations to determine the mineral compositions.

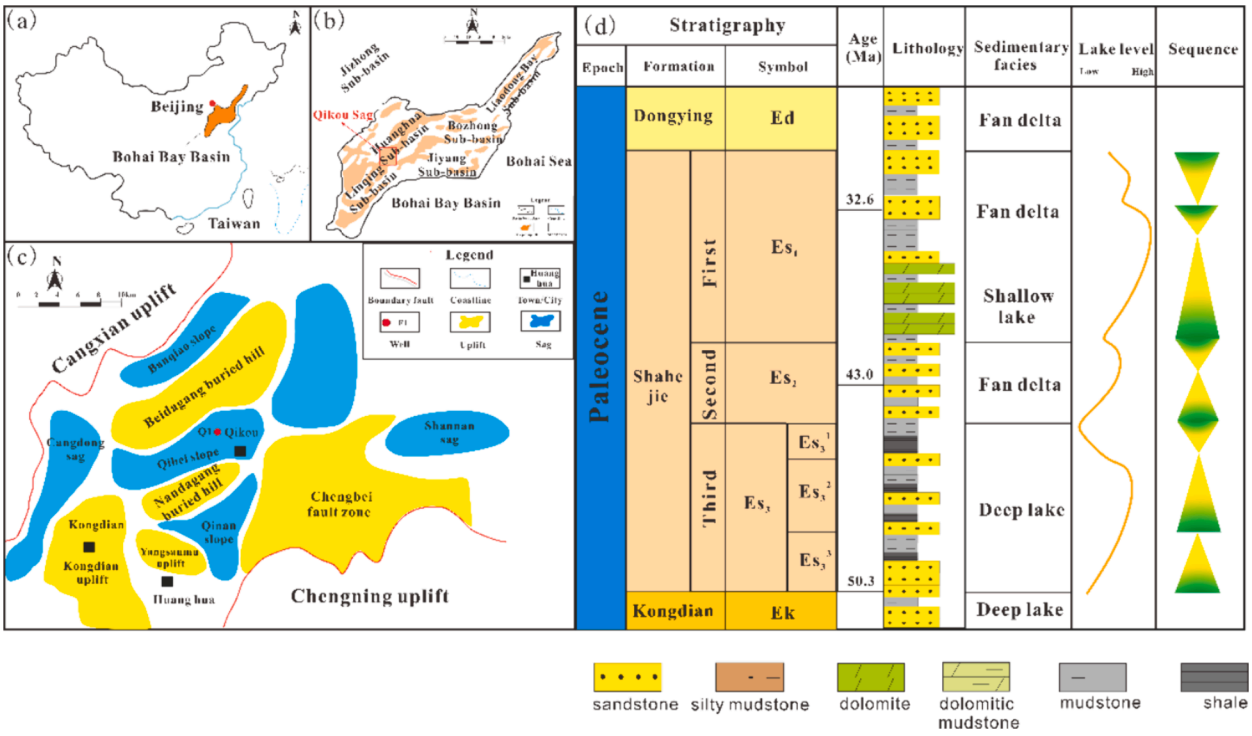

Fig. 1. The maps showing (a) the locations of Bohai Bay Basin; (b) the secondary tectonic units and location of the Qikou Sag in the Huanghua Depression; (c) the location of well Q1 for core samples; and (d) the diagram showing the stratigraphic compositions, main lithology, sedimentary facies, and sequence.

Concerning the thin section analysis, rock samples were polished or ground to create thin sections. These sections were then examined under single and orthogonal polarizations at magnification levels ranging from 20x to 400x.

Shale samples were prepared by polishing them with argon ion using Ilion 697. The polishing process took roughly two hours. The FEI Quanta FEG450 field emission scanning electron microscope was employed to examine shale samples polished with the argon ion using Ilion 697. This examination allowed for the determination of pore properties. It is important to note that the shale samples were polished for approximately two hours, while the microscope used a minimum visible aperture of 2 nm.

2.2.2. *Total organic carbon (TOC), and rock-eval pyrolysis*

To effectively conduct the total organic carbon analysis, the assessed sample size was reduced to a range of 170–200 mesh. After being neutralized with distilled water, inorganic carbon was removed from the samples using a 12.5 % hydrochloric acid solution and were subsequently dried at 60–80 °C in an oven. The quantity of TOC in the treated powdered samples was then measured.

The following method focused on pyrolysis through an instrument called the Rock-Eval. Initially, all samples were ground into a powder with a mesh size of 100, with 80 mg of each sample being added to the instrument and subsequently heated to 650 °C in a nitrogen-heavy environment at a rate of 25 °C per minute. The Rock–Eval pyrolysis instrument has the parameters of T_{max}, S_1 and S_2. The target temperature was set as 300 °C for 3 min and continued heating at 25 °C per min until reaching 650 °C. T_{max} constitutes the temperature for kerogen cracking, S_1 represents the quantity of free hydrocarbons under 300 °C, while S_2 represents the number of hydrocarbons produced from the kerogen cracking between the temperatures 300 °C and 650 °C.

2.2.3. *N_2 Adsorption, solvent extraction, fractionation, and gas chromatography–mass spectrometry (GC–MS)*

To effectively assess the N_2 adsorption and desorption, an ASAP 2460 surface area and pore volume analyzer from Micromeritics were employed. Prior to testing, the samples were dried in a vacuum oven at 150 °C for eight hours. In further accordance with standard SY/T 6154-2019, the samples were sieved to produce grain sizes of 0.250–0.425 mm. 12 powder samples, with a size of 100 mesh, were used for the solvent extraction and fractionation. Chloroform was added to samples while being maintained at a temperature of 70 °C in the Soxhlet extractor for 48 h. Metallic copper was subsequently added to the mixture to remove natural sulfur. The collected extracts were separated into maltenes (organic solvent-soluble components) and asphaltenes using hexane.

The GC–MS analysis was included to retrieve data explaining the sterane and terpene biomarkers, and was performed on the saturates using an Agilent 6890 N-5975B system equipped with a DB-5 ms capillary column (30 m × 0.25 mm × 0.25 μm). An appropriate amount of n-hexane, approximately 20 mg, was added to the oil and left to precipitate for 24 h, thereby effectively removing asphaltene. The remaining components were then adsorbed through an alumina separation column and mixed with n-hexane, dichloromethane and n-hexane at a ratio of 1:2, as well as dichloromethane and methanol at a ratio of 93:7, in a sequential manner. These solvents individually have the ability to elute saturated hydrocarbons, aromatic hydrocarbons, and non-hydrocarbon components, respectively. The saturated hydrocarbon components are subsequently subjected to the parameters of the GC–MS analysis using a GC–MS coupled instrument (Agilent-7890B/5977B MSD) for analysis and detection.

2.2.4. *T_1-T_2 NMR, confocal laser scanning microscopy, and multi-temperature pyrolysis*

The T_1-T_2 NMR tests were conducted at a temperature of 20 °C, where the first stage is focused on performing T_2 detection to determine the total amount of ^{1}H-containing compounds in the sample of shale. The equipment employed was calibrated specifically for the detection of ^{1}H-containing compounds. Following this, the T_1-T_2 NMR experiment was conducted to obtain a T_1-T_2 spectrum and quantitatively separate various substances.

Confocal Laser Scanning Microscopy was completed with the SP8

model to analyze at a micron scale the occurrence state of laminated shale oil, achieving a resolution of approximately 200 nm. The shale samples were sliced to a diameter of 0.04–0.05 mm for observation during the experiments at 25 °C, and 30–46 % relative humidity.

To conduct the multi-temperature pyrolysis, collected samples of powdered shale were heated at a rate of 25 °C per minute when reaching respective temperature intervals. To detect the product $S'_{1\text{-}1}$, the temperature was raised to 200 °C and held for one minute. After one minute at 200 °C, the samples were raised to 350 °C and again held at this temperature to detect the product $S'_{1\text{-}2}$. To detect the product $S'_{2\text{-}1}$, the temperature was raised to 450 °C and maintained for one minute. Finally, to identify product $S'_{2\text{-}2}$, the temperature was raised to 600 °C and held for a minute. $S'_{1\text{-}1}$ is primarily comprised of a light oil component existing in a free state. $S'_{1\text{-}2}$ consists mainly of light to medium oil components, which are also present in a free state. $S'_{2\text{-}1}$, however, encompasses heavy oil and colloidal asphaltene components, coexisting with organic matter in an adsorbed-mutually soluble state. $S'_{2\text{-}2}$ is comprised of hydrocarbons regenerated by kerogen pyrolysis within shale.

3. Results

3.1. Organic and inorganic composition of laminated shale

The mineralogical analysis results achieved from the shale samples are presented in Fig. 2**a**. Based on the results, the Es_3 shale samples are comprised of various mineral components including quartz, feldspar, clay (primarily chlorite and illite), calcite, and dolomite. A clear vertical heterogeneity in the mineral composition can also be observed within the samples. According to the classification of shale lithofacies [62,63], the Es_3 shale primarily belongs to the classification of mixed shale. The average TOC content level displayed by the shale samples ranges from 0.88 % to 2.59 %. Due to their hydrocarbon generation potential falling within the range of 2.12 to 11.78 mg/g, these samples can also be identified as excellent source rocks, with the data points specifically placing them in the medium and good source rock classification zones within the cross-plot (Fig. 2**b**).

Results achieved under the microscope revealed observable sedimentary laminae structures (Fig. 3**a, b**) comprised of various mineral compositions. The thickness of the laminae ranges from 20 to 100 μm (Fig. 3**c, f, i**), with the composition of dark laminae primarily consisting of clay and organic matter. The organic matter existent within the laminae exhibits a thickness of 10–65 μm and is primarily composed of an amorphous sapropelic matter. Algae are also occasionally discernible within the organic matter, exhibiting clear textures and fluorescence reactions (Fig. 3**d, g, j**). The clay minerals consisted of Illite and chlorite, which displayed continuous distribution (Fig. 3**h**). However, the bright laminae is mainly comprised of carbonate, felsic and other less prominent components (Fig. 3**e, h, k**). Pyrite, within the samples, is manifested in a strawberry-shaped distribution and manages to retain its crystal form (Fig. 3**k**), providing indication that the depositional environment is hypoxic in nature.

3.2. Characteristics of pore structures of laminated shale

The achieved shape of the N_2 adsorption–desorption curve serves as a reflection of the pore structure characteristics. According to the standards set by IUPAC classifications, the hysteresis loop of the N_2 adsorption–desorption isotherm curve is categorized into four types: H1, H2, H3, and H4 [64,65]. All Es_3 lacustrine shale samples exhibit hysteresis loops in their N_2 adsorption isotherms, indicating capillary condensation and evaporation processes, single-layer-multilayer adsorption, as well as micropore filling (Fig. 4). The results also revealed an important pattern where Sample 1, Sample 2, Sample 3, Sample 8, Sample 9, Sample 10, Sample 11and Sample 12 all demonstrated the characteristics of an H2 curve, which are defined by steep desorption curves and wide hysteresis loops, resembling an ink-bottle shape. Conversely, other samples exhibited the characteristics of an H3 curve, presented by narrow hysteresis loops and nearly parallel adsorption and desorption curves. When the samples were exposed to saturated vapor pressure conditions, capillary condensation occurred, resulting in a sharp rise in the adsorption level represented within the curve, indicative of parallel plate-like pores and slit-shaped pores.

3.3. Movable oil content detected by the multi-temperature pyrolysis and NMR T_1-T_2 map

According to the results recorded from the multi-temperature pyrolysis on movable oil content, the quantitative evaluation shows different characteristics of occurrence states, which are displayed in Fig. 5. The movable oil captured within $S'_{1\text{-}1} + S'_{1\text{-}2}$ ranged from 0.36 to 5.89 mg/g, with an overall average of 2.36 mg/g, which is much higher than the movable oil contents by Rock-Eval pyrolysis. Furthermore, the percentage level of movable oil $((S'_{1\text{-}1} + S'_{1\text{-}2})/(S'_{1\text{-}1} + S'_{1\text{-}2} + S'_{2\text{-}1} + S'_{2\text{-}2}))$ ranged from 40.18 % to 67.12 %, achieving an average of 50.97 %. These results show that the overall proportion of movable oil is relatively high compared to the levels recorded during the completion of the Rock-Eval pyrolysis. The proportion of indicated adsorbed oil, however,

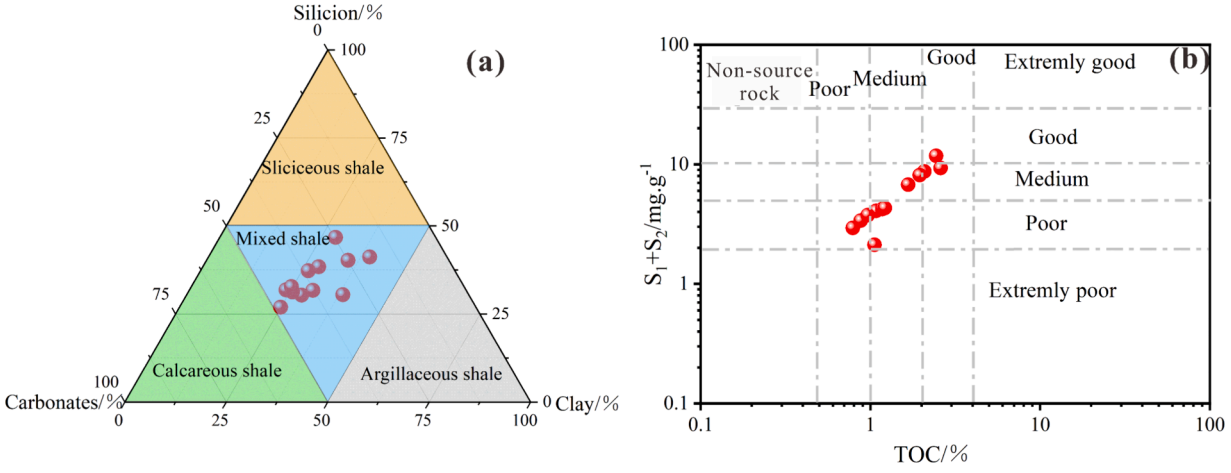

Fig. 2. Organic and inorganic composition characteristics of laminated shale. (a) Ternary diagram showing the relative abundance of inorganic minerals, i.e., silicon, carbonates and clay; (b) cross plot of TOC and $S_1 + S_2$. Silicion: quartz + feldspar; Carbonates: calcite + dolomite. TOC, Total Organic Carbon; S_1, volatile hydrocarbons at 300 °C from Rock-Eval experiments, S_2: kerogen-derived hydrocarbons between 300 °C and 550–650 °C from Rock-Eval experiments.

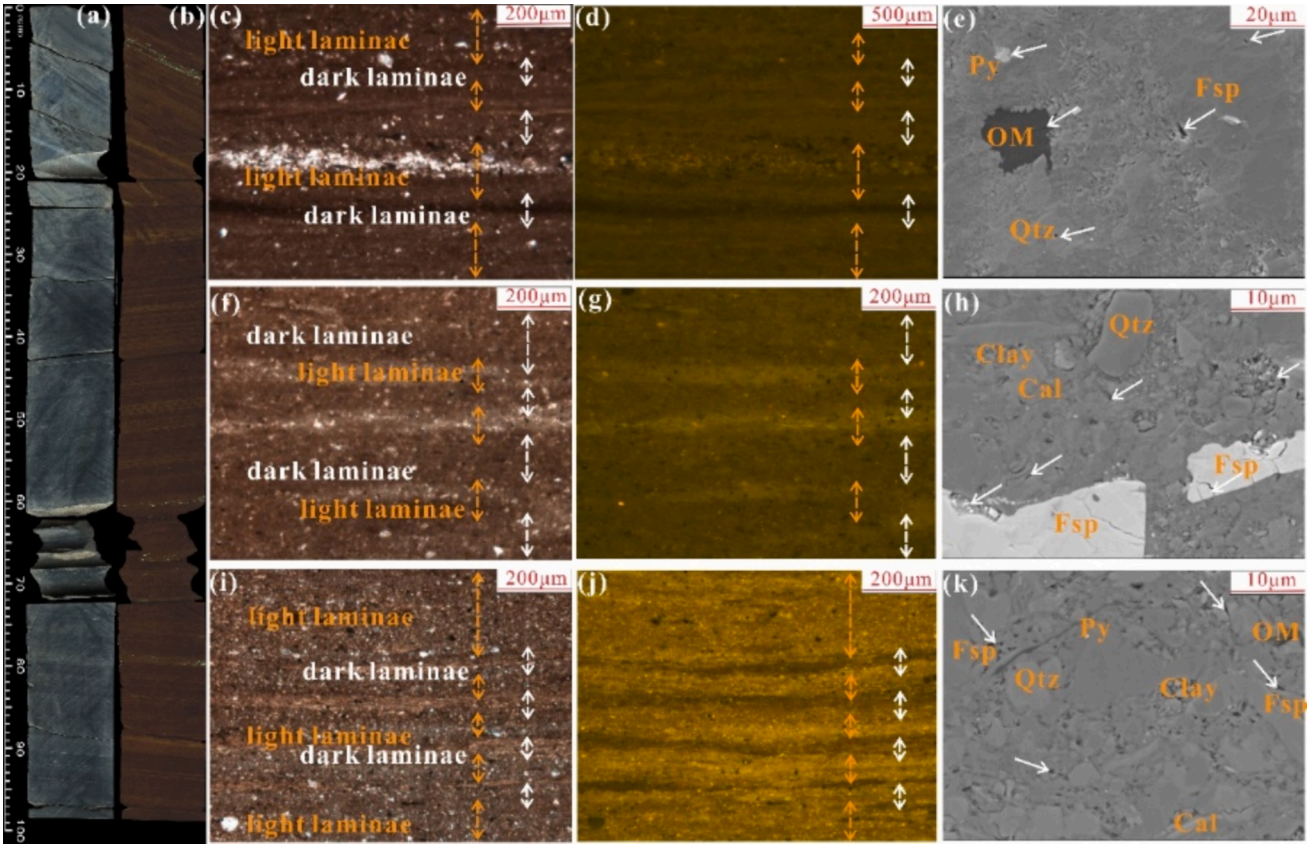

Fig. 3. Petrographic characteristics of the organic-rich shale in the 3th member Shahejie Formation from the well Q1 in the study area. (a) Core column showing the laminae development characteristics from 3996.74 to 3997.74 m in general optical scanning. (b) Core column showing the laminae development characteristics from 3996.74 to 3997.74 m in fluorescence scanning. (c) Low-frequency lamina showing the lamina interval of light and dark laminas, well Q1,3988.64 m. (d) Fluorescence thin sections under fluorescence light to show fluorescence characteristics in low-frequency laminae, well Q1,3988.64 m. (e) An SEM image, illustrating that OM grow around rigid particles of quartz, feldspar, and pyrite, well Q1,3988.64 m. (f) Medium-frequency lamina showing the lamina interval of light and dark laminas, well Q1,3990.86 m. (g) Fluorescence thin sections under fluorescence light to show fluorescence characteristics in medium-frequency laminae, well Q1, 3990.86 m. (h) An SEM image, illustrating that the clay, quartz, feldspar and calcite develop, well Q1, 3990.86 m. (i) High-frequency lamina showing the lamina interval of light and dark laminas, well Q1,4046.83 m. (j) Fluorescence thin sections under fluorescence light to show fluorescence characteristics in high-frequency laminae, well Q1, 34046.83 m. (k) An SEM image, illustrating that clay and OM grow around quartz, feldspar, and pyrite, well Q1, 4046.83 m. Py, Pyrite; Qtz, Quartz; OM, Organic matter; Fsp, Feldspar; Cal, Calcite.

shows a decreasing trend, corresponding to a relatively high overall proportion of light movable oil. $S'_{1\text{-}1}$ is primarily comprised of a light oil component existing in a free state. The $S'_{1\text{-}1}$ ranged from 0.23 to 3.53 mg/g, with an overall average of 1.29 mg/g. The actual realized movable oil rate ($S'_{1\text{-}1}/(S'_{1\text{-}1} + S'_{1\text{-}2} + S'_{2\text{-}1} + S'_{2\text{-}2})$) ranged from 20.91 % to 43.01 %, achieving an average of 28.04 %, indicating that the sampled shale oil mainly exists in a movable state.

The longitudinal relaxation time (T_1) and transverse relaxation time (T_2) parameters, derived through the two-dimensional nuclear magnetic resonance (NMR) spectroscopic technique, offer significant insights into the relative quantities of swelling, adsorption, and movable oil in shale. When the two-dimensional T_1-T_2 NMR spectroscopic method is used to assess hydrocarbon occurrence, a quantitative analysis of shale oil concentration in various occurrence states can also be achieved [66,67]. As illustrated in Fig. 6 [68], the detectable movable oil content within these samples ranged from 3.96 to 7.05 mg/g, with an average of 5.36 mg/g. Additionally, through the observation of the T_1-T_2 spectra, clear boundaries can be seen that delineate movable oil, adsorbed oil, and free-water areas. Overall, a relatively high movable oil content is retained, indicating favorable overall fluidity.

3.4. Fractionation of movable oil from lamina

Saturates, aromatics, asphaltenes, and resins make up the composition of laminated oil. Different types of oil are composed of different components, which represent differences in their individual physical and chemical properties. Judging from the results retrieved from the component analysis, the percentage of saturates identified within the sample ranges from 16 % to 64 %, with an average value of 51 %, while the content of resins and asphaltenes range from 11 % to 37 %, with an average value of 51 %. It's evident that the characteristics of the components are marked by the predominance of saturates and aromatics (Table 1).

4. Discussion

4.1. Characterization of mobility in laminated shale oil

The Es_3 shale exhibits distinct fluorescence characteristics, primarily manifesting as medium-bright orange and yellow color, indicative of various asphaltic fractions including colloidal asphalt and asphaltene asphalt (Fig. 7). With regard to the results achieved from laminated shale oil reservoirs, the dark laminae predominantly displayed a green fluorescence with diminished luminosity, as well as a compositional prevalence of heavy components (Fig. 7**a**). Conversely, the bright laminae can be signified by a medium-bright fluorescence, with asphalt predominantly situated within the intergranular pores of felsic minerals, and the dissolution pores of carbonate minerals. These regions in

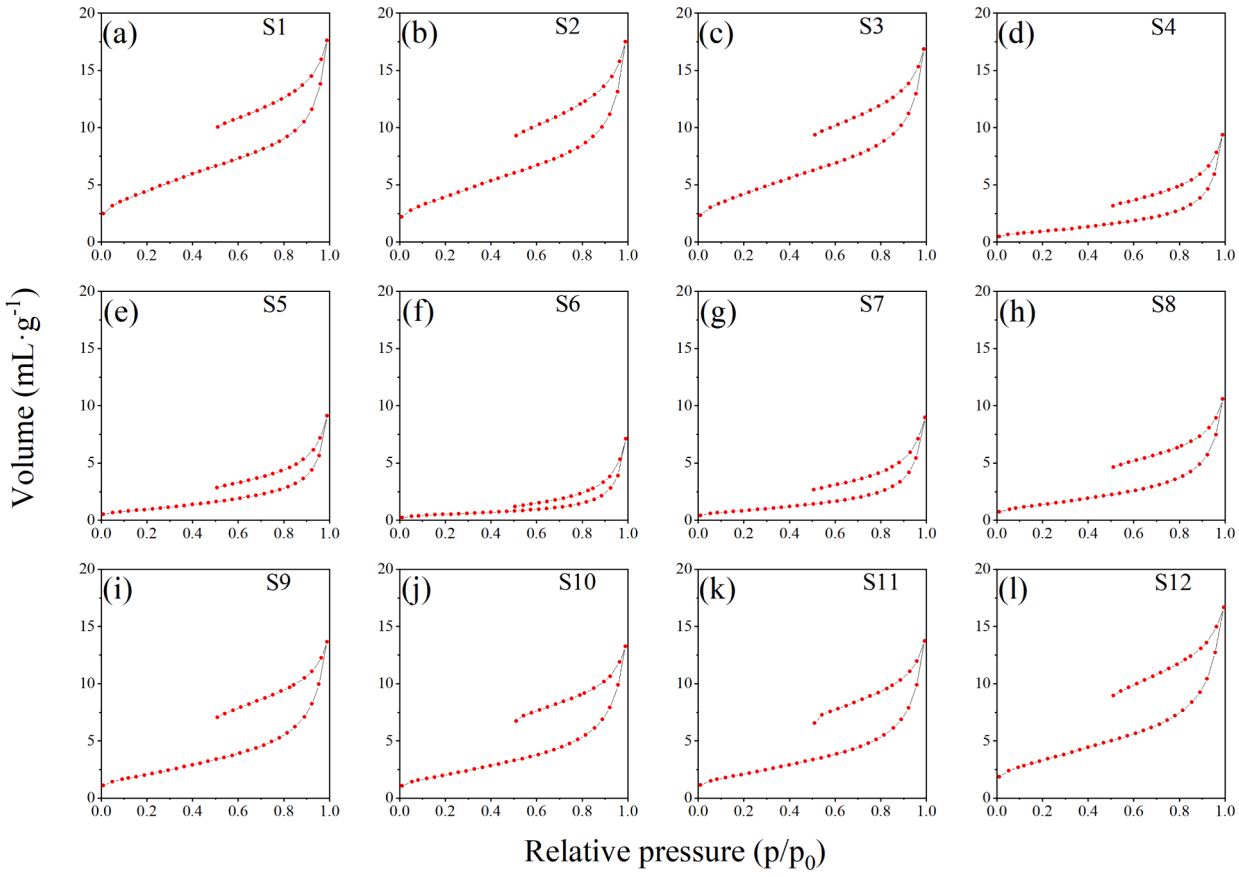

Fig. 4. Typical N_2 curves showing the pore structure of laminated shale. Sample 1, Sample 2, Sample 3, Sample 8, Sample 9, Sample 10, Sample 11and Sample 12 shows a similar distribution and can be together. Others shows a similar distribution. N_2 adsorption–desorption isotherms for selected (a, b, c, h, i, k, l) samples showing a H2 curve characteristic and (d–g) showing a H3 curve characteristic.

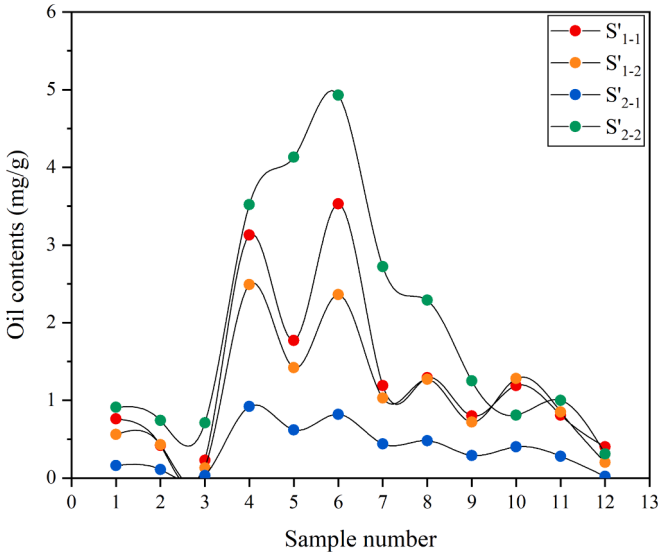

Fig. 5. Different oil contents of laminated shale samples from multi-temperature pyrolysis. S'_{1-1}, $S'_{1-1} + S'_{1-2}$, S'_{2-1} and S'_{2-2} represent the content of actual movable oil, maximum movable oil, adsorbed oil and kerogen cracking oil.

particular exhibit a heightened abundance of dark yellow fluorescence, which can be primarily attributed to the characteristic of oily asphalt and supplemented by asphaltene asphalt. Additionally, it is evident that the bright laminae better facilitate movable oil content, while also enhancing overall mobility, in comparison to dark laminae (Fig. 7**b**). The confocal laser scanning microscopy technique was also able to delineate the pattern distribution of light and heavy components primarily within matrix pores into a classification of diffuse patterns (Fig. 7**c, d**). However, within lamina-dominated regions, both light and heavy oil tend to accumulate, with heavy oil exhibiting a propensity to be absorbed into the laminae surfaces. This phenomenon can be chiefly attributed to the concentration of heavy components within select organic matter or clay-rich dark laminae. However, light components are partially sequestered within intergranular or dissolution pores of brighter laminae.

Differences in the level of detectable movable oil content recorded by different analytical methods is shown in Fig. 8**a**. Through the Rock–Eval pyrolysis, S_1 denotes the hydrocarbons liberated from the shale upon being heated to a temperature of 300 °C, leaving a portion of generated hydrocarbons yet to be expelled. S_1 exhibits a movable oil content ranging from 0.57 to 3.29 mg/g, averaging 1.41 mg/g, indicating a relatively high concentration of movable oil. When evaluating the results achieved from the multi-temperature pyrolysis, $S'_{1-1} + S'_{1-2}$ signifies the recorded level of movable oil. The movable oil ($S'_{1-1} + S'_{1-2}$) content recorded within these shale samples ranges from 0.36 to 5.89 mg/g, with an average of 2.36 mg/g. The percentage of movable oil varied from 40.18 % to 67.12 %, achieving an averaging of 50.97 %. Consistent with the previously mentioned pyrolysis results, the overall proportion of movable oil is relatively high. Results recorded from the T_1-T_2 NMR experiments indicate a level of movable oil content ranging from 3.96 to 7.05 mg/g, with an average of 5.36 mg/g. In this instance, a higher proportion of movable oil signifies favorable overall fluidity.

When comparing the various levels of movable oil content recorded by the different analytical methods, the level determined through the

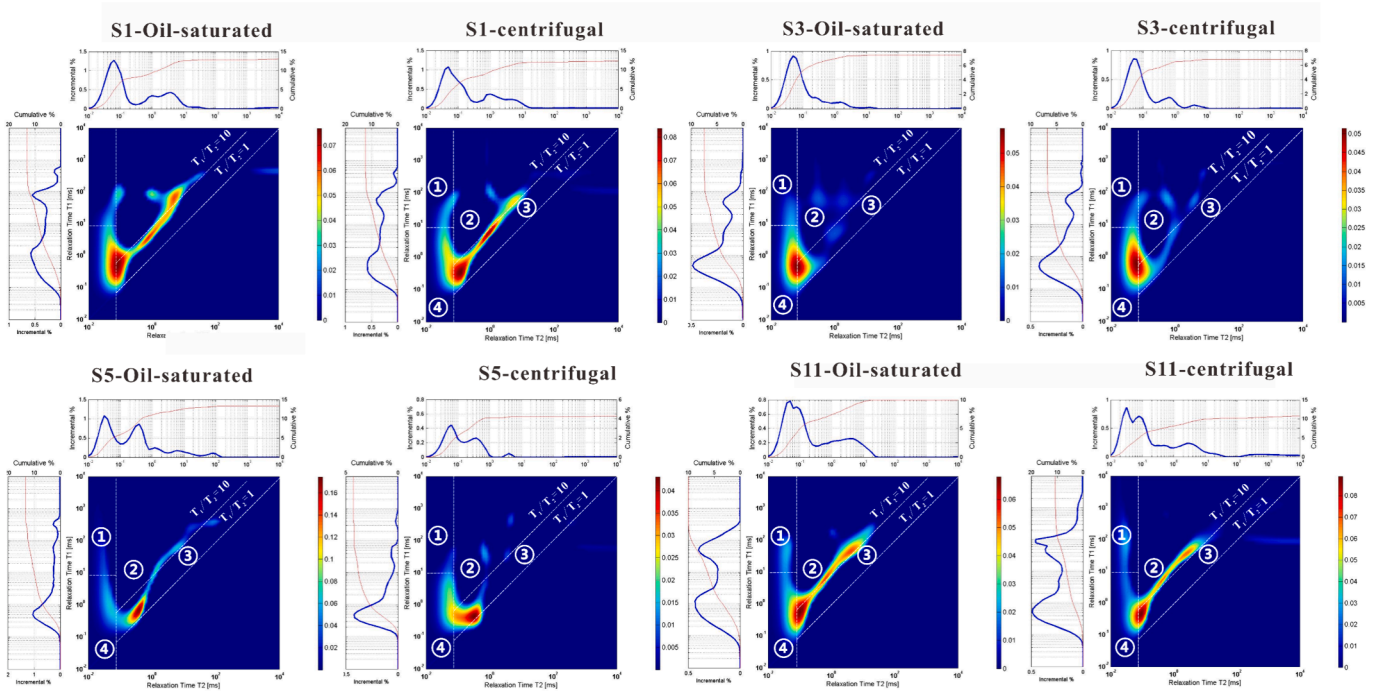

Fig. 6. Locations and NMR tests results of each hydrogen-bearing components of typical laminated shale samples. (Regions ① to ④ successively represent kerogen/solid bitumen, movable oil, free/adsorbed water,structural water, respectively).

Table 1
Component separation of the movable oil from laminated shale.

Sample number	Saturates/%	Aromatics/%	Resins/%	Asphaltenes /%	Carbon distribution	Peak carbon	CPI	nC_{21}-/nC_{22}+
1	48.98	19.87	12.68	3.60	17–36	23	1.03	0.16
2	13.47	61.20	7.63	2.11	17–36	23	1.04	0.17
3	46.94	24.28	10.97	2.70	17–36	23	1.05	0.19
4	49.77	20.33	11.38	3.19	17–36	25	0.99	0.24
5	48.93	18.63	12.52	3.98	17–36	22	1.01	0.28
6	39.01	34.58	9.52	1.88	17–36	22	0.96	0.31
7	31.75	39.56	12.39	2.21	17–36	23	1.02	0.23
8	50.42	13.20	13.76	22.61	17–36	23	1.01	0.22
9	56.96	15.57	14.98	12.50	11–38	17	0.99	0.21
10	63.77	12.21	12.62	11.40	14–38	17	0.98	0.23
11	62.31	15.51	11.29	10.88	12–38	17	1.02	0.22
12	53.86	15.59	12.22	18.33	12–38	17	1.01	0.19

Carbon preference index (CPI) $= \frac{\left(\sum_{i=n}^{m} C_{2i+1}\right) + \left(\sum_{i=n+1}^{m+1} C_{2i+1}\right)}{2\left(\sum_{i=n+1}^{m+1} C_{2i}\right)}$; where n is the starting n-alkane divided by 2 and m is the ending nalkane divided by 2.

Rock–Eval pyrolysis experiments was found to be approximately 40–50 % lower than the results obtained from multi-temperature pyrolysis (Fig. 8**b**) and T_1-T_2 NMR experiments. This result indicates that before the pyrolysis experiment, approximately 50–60 % of the movable hydrocarbons existent within the laminated shale had already been lost throughout the process [69,70]. During the crushing stage of the shale sample preparation, the pyrolysis experiment experiences a rapid loss of originally retained gaseous and light hydrocarbons. The loss of light hydrocarbons is drastically exacerbated during this process compared to natural circumstances, leading to a decrease in the mobile oil content [71,72] Movable oil content is also lost during the time that samples are sent to the pyrolysis equipment prior to the commencement of testing.

Variations could also be observed between the results obtained from the multi-temperature pyrolysis and the T_1-T_2 NMR experiments. Discrepancies in the lower limits of relaxation time among various states can result in differences in the recorded level of movable oil content, leading to evident analytical inaccuracies. Furthermore, variations also exist with regard to the relaxation rates observed among different pores. Consequently, many significant uncertainties remain when interpreting the results of the T_1-T_2 NMR experiment, leading to disparities between the two methodologies.

4.2. Compositional characteristics of movable oil in laminated shale

The development process of laminae seems to significantly influence the compositional characteristics of movable oil (Fig. 9). This relationship helps us understand that while the compositions of movable oil in Samples 1 and 12 are comparable (Fig. 9**a, d**) with regard to their saturates content, noticeable differences exist in the distribution characteristics of said saturates. Sample 1 exhibits a carbon number distribution ranging from 17 to 36 (Fig. 9**b**), with a primary peak at C_{23} and a CPI of 1.03 (Table1), whereas sample 12 displays a carbon number distribution between 12 and 38 (Fig. 9**e**), with its respective primary peak at C_{17} and a CPI of 1.01 (Table1). The spectra achieved for samples 1 and 12 indicate the complete absence of hydrocarbons lighter than C_{12}. However, many noticeable differences remain (Fig. 9**c, f**). For

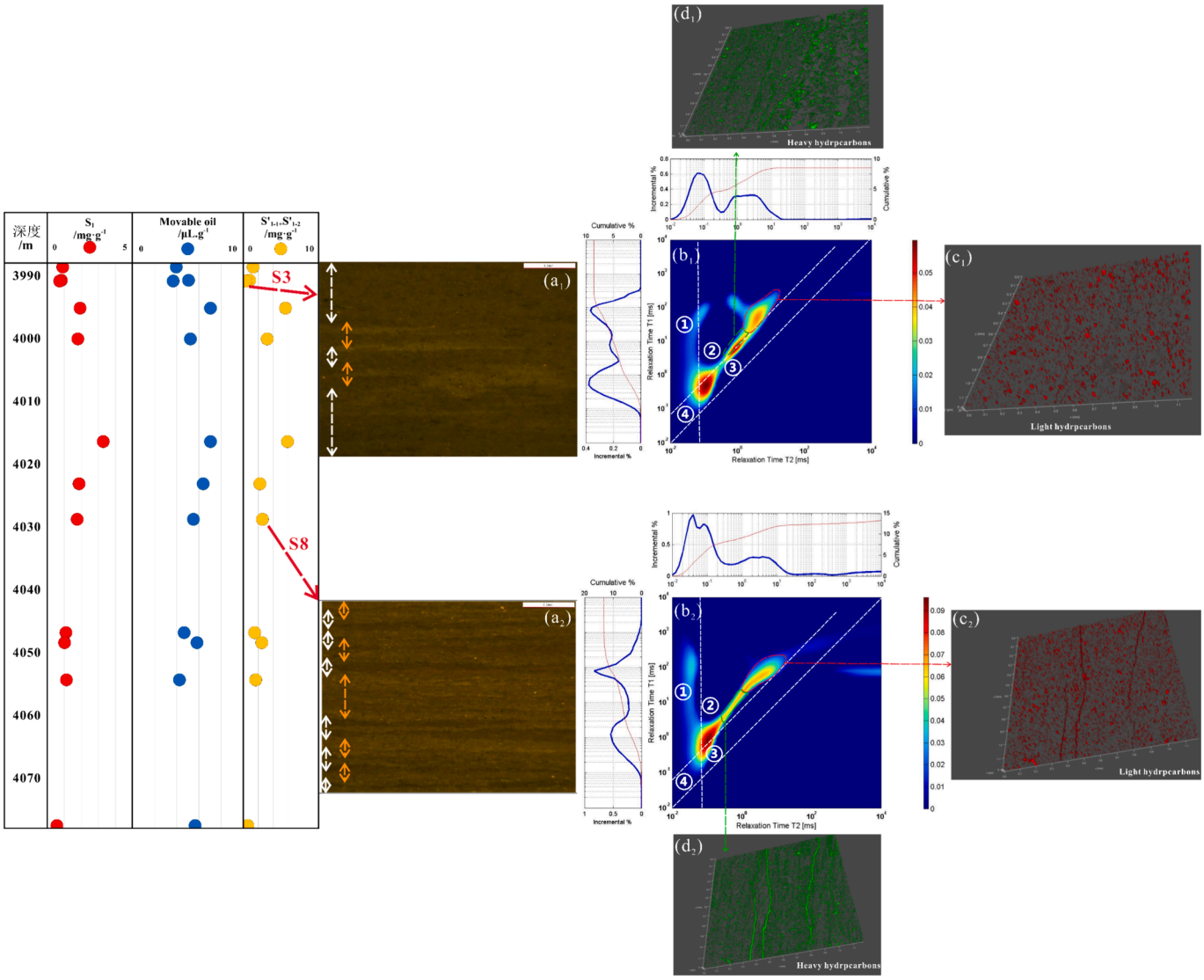

Fig. 7. Movable oil contents and distribution characteristics of the laminated shale. (a_1) Fluorescence thin sections under fluorescence light to show fluorescence characteristics in low-frequency laminae, well Q1, 3990.86 m. (b_1) NMR T_1-T_2 map of sample S3 with low-frequency laminae, well Q1, 3990.86 m. (c_1) Occurrence characteristics of heavy oil in low-frequency laminae, well Q1, 3990.86 m. (d_1) Occurrence characteristics of light oil in low-frequency laminae, well Q1, 3990.86 m. (a_2) Fluorescence thin sections under fluorescence light to show fluorescence characteristics in high-frequency laminae, well Q1, 4028.79 m. (b_2) NMR T_1-T_2 map of sample S8 with high −frequency laminae, well Q1, 4028.79 m. (c_2) Occurrence characteristics of heavy oil in high-frequency laminae, well Q1, 4028.79 m. (d_2) Occurrence characteristics of light oil in high-frequency laminae, well Q1, 4028.79 m.

example, sample 12 exhibits laminae development, with a primary peak of carbon at C_{17}, which is notably smaller than the peak achieved by sample 1 at C_{23}, suggesting that the development of laminae may facilitate the enrichment and retention of lighter components.

4.3. Controlling factors on laminated shale oil mobility

To precisely assess the factors influencing movable oil contents, this study conducted a correlation heat map analysis, with the results being depicted in Fig. 10. Movable oil content exhibits a positive correlation with the level of total organic carbon (TOC), carbonate minerals content, pore size, and the nC_{21}-/nC_{22} + ratio. Notably, pore size seems to exert the most substantial positive influence on the level of movable oil content, evidenced by a correlation coefficient of 0.79. Conversely, the level of movable oil content demonstrated a negative correlation with total clay content, specific surface area, and the carbon preference index (CPI). Remarkably, the factor of specific surface area exhibits the most significant negative impact on movable oil content among these factors.

The results achieved also demonstrated that the fundamental basis for hydrocarbon production lies in the quantity of organic matter that exists. As a result, shale oil reaches its absorption capacity limit as total organic carbon (TOC) increases. Thus, remnants remain within the shale pores and fractures, consequently leading to a gradual increase in the volume of movable oil.

Mineral composition was also proved to significantly influence the mobility of shale oil. Results showed that clay content negatively impacts movable oil due to the sheet-like structure of clay minerals, its large specific surface area (Fig. 11**a**), and its strong affinity for oil adsorption. Conversely, quartz and dolomite better facilitate and enrich the mobility of oil. Mineral dissolution provides the spatial groundwork for movable oil accumulation, while dolomite's strong polarity allows for the greater ease in terms of the absorption of polar substances (Fig. 11**b**) [27]. Upon contact with oil, dolomite surfaces exhibit lipophilic characteristics, thereby enhancing the potential level of movable oil content (Fig. 11**c**).

It must also be noted that the characteristics of shale reservoirs

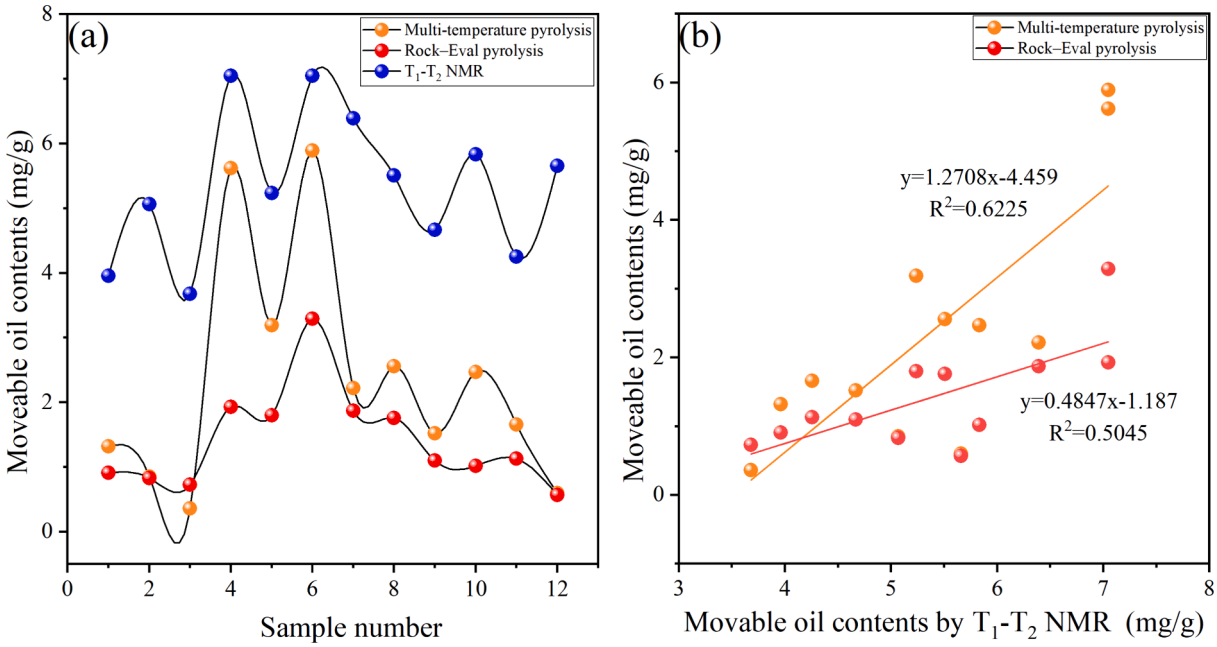

Fig. 8. Movable oil contents and the relationship of the lacustrine shale samples. (a) The difference of movable oil contents characterized by multi-temperature pyrolysis, Rock–Eval pyrolysis, T_1-T_2 NMR; (b) cross plot showing a linear relationship between movable oil contents by multi-temperature pyrolysis, Rock–Eval pyrolysis and movable oil contents by T_1-T_2 NMR.

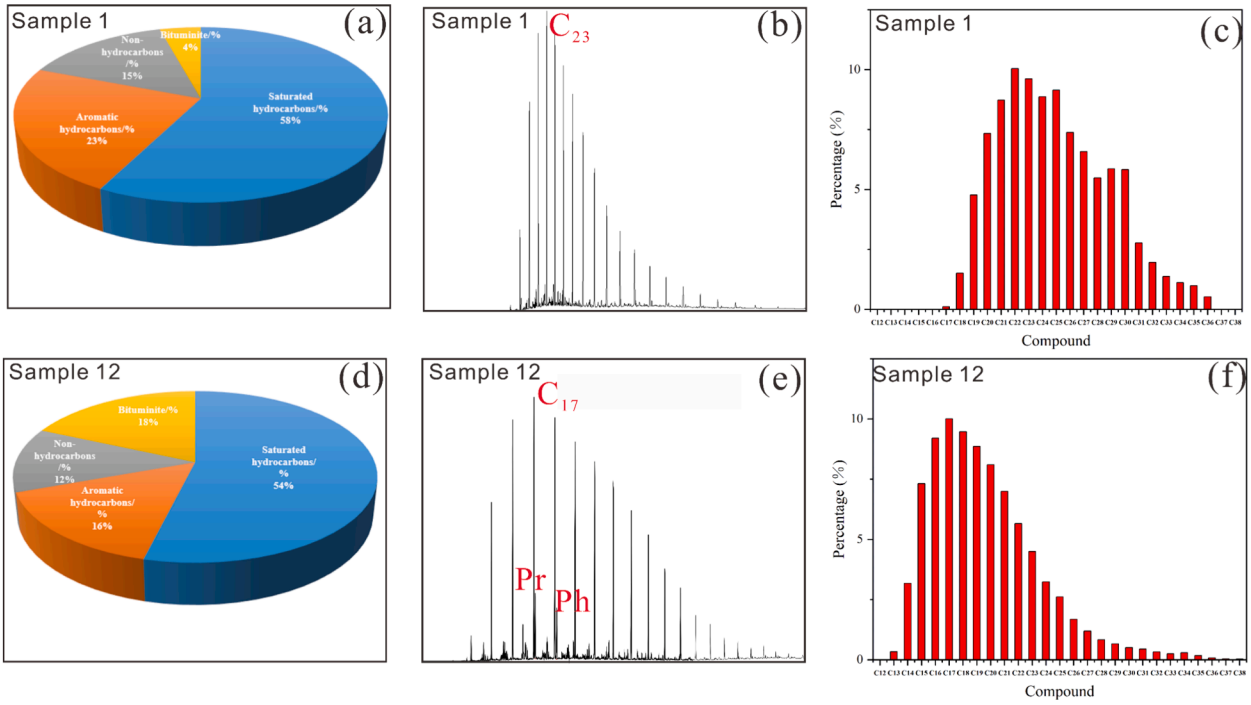

Fig. 9. Composition characteristics of movable oil in laminae of the shale samples. (a) Chemical component content of movable oil in low-frequency laminae from Sample 1, well Q1, 3988.64 m; (b) Typical mass chromatograms of *m/z* 85 of movable oil in low-frequency laminae from Sample 1, well Q1, 3988.64 m; (c) Normal alkane with different carbon number of movable oil in low-frequency laminae from Sample 1, well Q1, 3988.64 m;(d) Chemical component content of movable oil in high-frequency laminae from Sample 12, well Q1, 4077.56 m;(e) Typical mass chromatograms comparison of *m/z* 85 of movable oil in high-frequency laminae from Sample 12, well Q1, 4077.56 m; (f) Normal alkane with different carbon number of movable oil in high-frequency laminae from Sample 12, well Q1, 4077.56 m. Pr, Pristane; Ph, Phytane.

predominantly influence the level of movable oil in shale. The shale pore system is primarily comprised of inorganic pores, accounting for 81 % of potential storage capacity (Fig. 11**d**). Pores that have diameters ranging from 100 to 500 nm contribute significantly to storage ability (Fig. 11**e**). Well-developed pores, such as intergranular and dissolution pores, exhibit superior fluorescence responses (Fig. 11**f**), particularly when formed in bright laminae, which attributes to their broader range of pore diameter, providing ample storage space and flow channels. Conversely, fluorescence within dark laminae tends to become subdued (Fig. 11**g**).

Another important factor to highlight is the difference in distribution

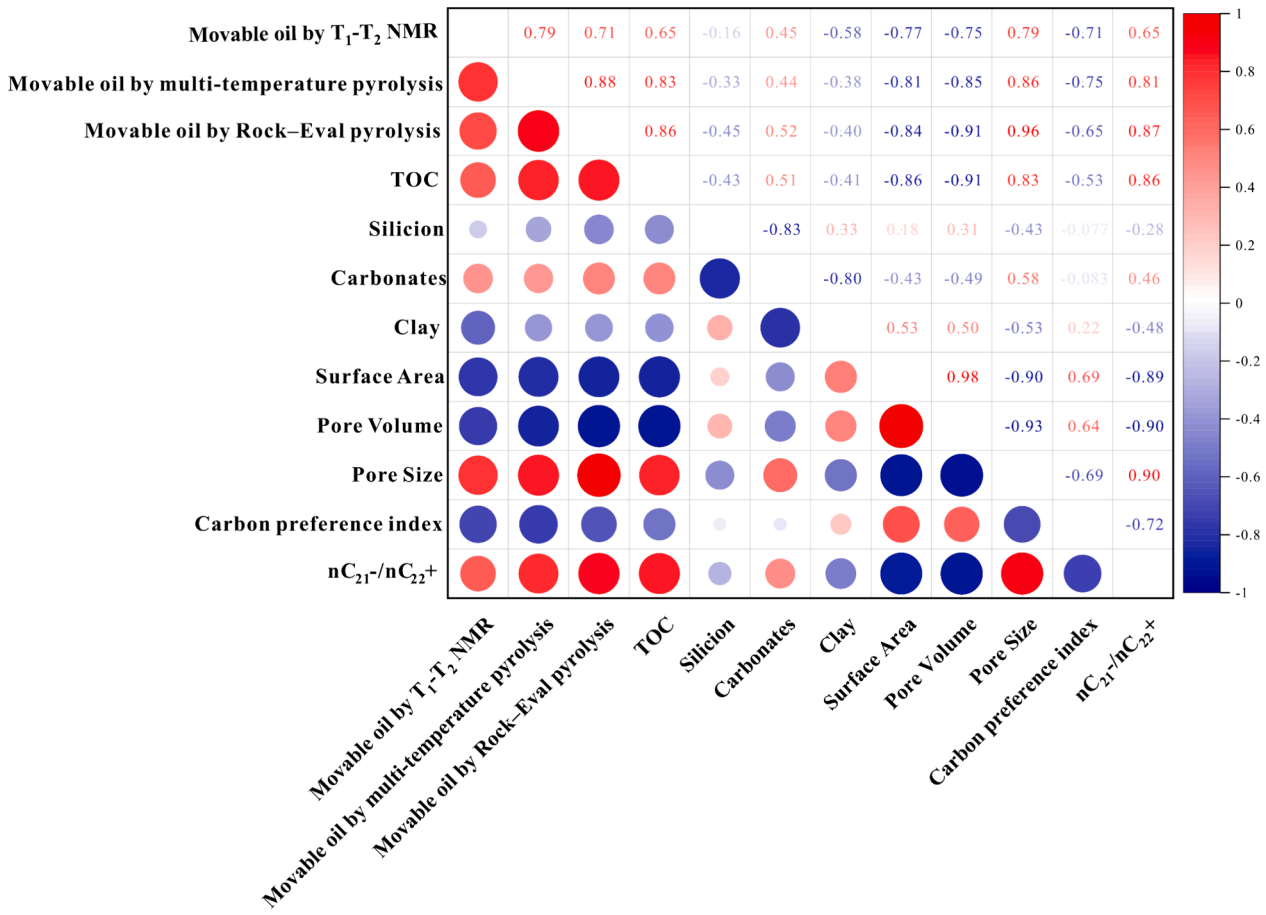

Fig. 10. Correlation heatmap of shale samples in geochemical, mineral, and pore characteristics with mobility parameters of the lacustrine shale samples.

characteristics of movable oil within bright and dark laminae. In dark laminae, light components predominate over heavy components, typically forming elongated strips along bedding planes (Fig. 11h). This occurrence is primarily due to light components migrating when placed under pressure from the process of hydrocarbon generation. Additionally, micro-migration is facilitated by capillary pressure, leading to the preferential discharge of light components into light laminae. Such components include substances such as felsic or carbonate, which become enriched, while heavy components remain dispersed and become absorbed onto kerogen surfaces, predominantly influenced by the distribution of organic matter (Fig. 11**i**).

5. Conclusion

If the evaluation of mobile oil within laminated shale structures is conducted inaccurately it will significantly restrict the estimated ultimate recovery. This study began by comprehensively evaluating the heterogeneity on the mobility of shale oil and controlling factors between bright laminae and dark laminae. To demonstrate the heterogeneity characteristics among different laminae, an analysis was conducted on the mobility of laminated shale oil in the Paleogene Shahejie Formation of Bohai Bay Basin. The results achieved from this research should improve our ability to characterize oil mobility and exploit laminated shale oil sweet spots. It has generally been considered that laminated shale reservoirs tend to have a lower estimated ultimate recovery. However, based on the findings of this paper, this may not always be the case.

This paper determined that movable oil tends to be mainly stored within bright laminae rather than dark laminae, due primarily to the process of migration from dark laminae to bright laminae. Thus, bright laminae within shale oil reservoirs may contribute to the formation of sweet spots for shale oil production. It was also demonstrated that movable oil is mainly stored in pores with diameters reaching 100–500 nm of bright laminae, while previous studies have tended to indicate that smaller pores with diameters of 20–200 nm contribute more significantly to shale oil production. Due to the volatility of light hydrocarbons and experiment conditions, this paper also determined that the movable oil contents analyzed by T_1-T_2 NMR were significantly more reliable than those achieved by the Rock-Eval pyrolysis and multi-temperature pyrolysis methods. This research was able to provide corresponding geological examples during the process of analysis. However, this paper through attempting to use molecular dynamics simulation was unable to reveal the flowing mechanisms of movable oil from the micro to nanoscale perspective. These dynamics may also affect oil mobility during thermal maturation. Hence, this should be a focus area of future studies.

CRediT authorship contribution statement

Biao Sun: Writing – original draft, Visualization, Validation, Methodology, Investigation, Funding acquisition, Data curation. **Xiaoping Liu:** Writing – review & editing, Funding acquisition. **Xianzheng Zhao:** Writing – review & editing, Resources. **Murray Gingras:** Writing – review & editing. **Fengming Jin:** Writing – review & editing, Resources. **Tian Liu:** Methodology, Investigation, Data curation. **Zuxian Hua:** Visualization, Software. **Wendi Peng:** Data curation. **Yu Yuan:** Investigation.

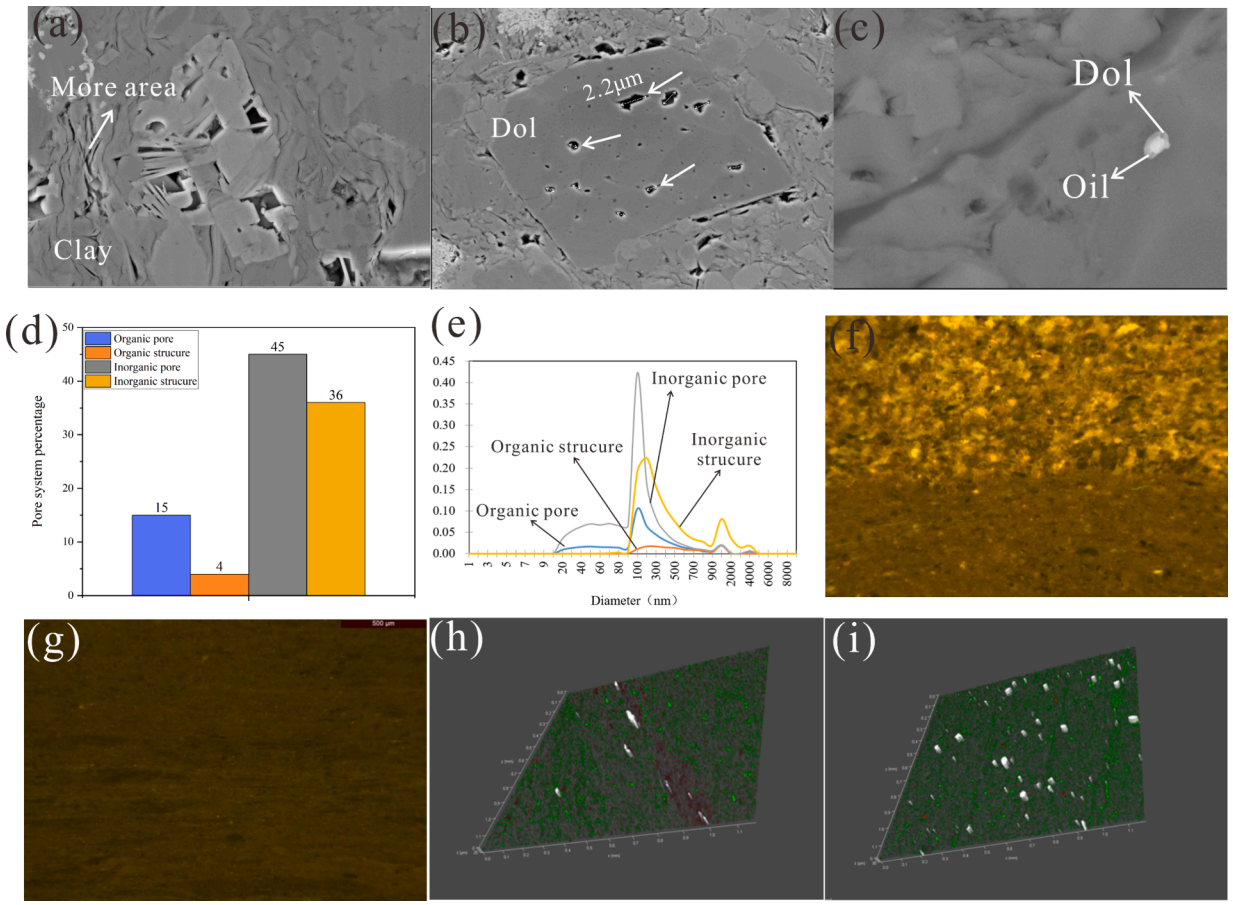

Fig. 11. The controlling factors of movable contents in TOC, mineral composition, pore characteristics and laminae. (a) Microfractures of clay minerals have larger surface area, well Q1, 4046.83 m; (b) Dissolution pores of dolomites add the storge of movable oil, well Q1, 4077.56 m; (c) The dolomite is absorbed by movable oil, well Q1, 4016.43 m; (d) The dolomite is absorbed by movable oil, well Q1, 4016.43 m; (d) The percentage of different pore styles of laminated shale, well Q1, 4028.79 m; (e) The pore diameter distribution characteristics of different pore styles of laminated shale, well Q1, 4028.79 m; (f) Fluorescence thin sections under fluorescence light shows movable oil is in high-frequency laminae, well Q1, 4054.36 m; (g) Fluorescence thin sections under fluorescence light shows movable oil is in low-frequency laminae, well Q1, 4048.44 m; (h) Light movable oil distributed in lamina, well Q1, 3995.18 m; (i) Heavy movable oil distributed randomly, well Q1, 3990.74 m. (White, minerals; red, light oil; green, heavy oil).

Declaration of competing interest

The authors declare that they have no known competing financial interests or personal relationships that could have appeared to influence the work reported in this paper.

Data availability

Data will be made available on request.

Acknowledgments

This work was financially supported by the National Natural Science Foundation of China (Grant No. 42072150) and we thank the sponsors of this project.

References

[1] Hu S, Zhao W, Hou L, Yang Z, Zhu R, Wu S, et al. Development potential and technical strategy of continental shale oil in China. Pet Explor Dev 2020;47:877–87. https://doi.org/10.1016/S1876-3804(20)60103-3.
[2] Gao Z, Bai L, Hu Q, Yang Z, Jiang Z, Wang Z, et al. Shale oil migration across multiple scales: a review of characterization methods and different patterns. Earth-Sci Rev 2024;254:104819. https://doi.org/10.1016/j.earscirev.2024.104819.
[3] Han W, Luo X, Tao S, Lin S, Liu J, Yang Y. Activation energy and organic matter structure characteristics of shale kerogen and their significance for the in-situ conversion process of shale oil. Fuel 2024;370:131823. https://doi.org/10.1016/j.fuel.2024.131823.
[4] Wang F, Chang S. Molecular dynamics investigation of shale oil occurrence and adsorption in nanopores: unveiling wettability and influencing factors. Chem Eng J 2024;481:148380. https://doi.org/10.1016/j.cej.2023.148380.
[5] Hu T, Liu Y, Jiang F, Pang X, Wang Q, Zhou K, et al. A novel method for quantifying hydrocarbon micromigration in heterogeneous shale and the controlling mechanism. Energy 2024;288:129712. https://doi.org/10.1016/j.energy.2023.129712.
[6] Pang X, Li M, Li B, Wang T, Hui S, Liu Y, et al. Main controlling factors and movability evaluation of continental shale oil. Earth-Science Rev 2023;243:104472. https://doi.org/10.1016/j.earscirev.2023.104472.
[7] Tian H, He K, Huangfu Y, Liao F, Wang X, Zhang S. Oil content and mobility in a shale reservoir in Songliao Basin, Northeast China: Insights from combined solvent extraction and NMR methods. Fuel 2024;357:129678. https://doi.org/10.1016/j.fuel.2023.129678.
[8] Li J, Jiang C, Wang M, Lu S, Chen Z, Chen G, et al. Adsorbed and free hydrocarbons in unconventional shale reservoir: a new insight from NMR T1–T2 maps. Mar Pet Geol 2020;116:104311. https://doi.org/10.1016/j.marpetgeo.2020.104311.
[9] Xiao F, Yang J, Li S, Yao Y, Huang Y, Gao X. Enrichment and movability of lacustrine tight shale oil for the first member of the Upper Cretaceous Qingshankou Formation in the Sanzhao Sag, Songliao Basin, NE China: insights from saturated hydrocarbon molecules. Fuel 2024;368:131615. https://doi.org/10.1016/j.fuel.2024.131615.
[10] Gou Q, Xu S. The controls of laminae on lacustrine shale oil content in China: a review from generation, retention, and storage. Energies 2023;16. https://doi.org/10.3390/en16041987.
[11] Liu Q, Li P, Jin Z, Sun Y, Hu G, Zhu D, et al. Organic-rich formation and hydrocarbon enrichment of lacustrine shale strata: a case study of Chang 7 Member. Sci China Earth Sci 2022;65:118–38. https://doi.org/10.1007/s11430-021-9819-y.
[12] Gao Z, Duan L, Jiang Z, Huang L, Chang J, Zheng G, et al. Using laser scanning confocal microscopy combined with saturated oil experiment to investigate the

pseudo in-situ occurrence mechanism of light and heavy components of shale oil in sub-micron scale. J Pet Sci Eng 2023;220:111234. https://doi.org/10.1016/j.petrol.2022.111234.
[13] Li S, Hu S, Xie X, Lv Q, Huang X, Ye J. Assessment of shale oil potential using a new free hydrocarbon index. Int J Coal Geol 2016;156:74–85. https://doi.org/10.1016/j.coal.2016.02.005.
[14] Yan G, Xu YH, Xu WL, Bai B, Bai Y, Fan YP, et al. Shale oil resource evaluation with an improved understanding of free hydrocarbons: Insights from three-step hydrocarbon thermal desorption. Geosci Front 2023;14:101677. https://doi.org/10.1016/j.gsf.2023.101677.
[15] Zhang P, Lu S, Lin Z, Duan H, Chang X, Qiu Y, et al. Key oil content parameter correction of shale oil resources: a case study of the paleogene funing formation, Subei Basin. China Energy and Fuels 2022. https://doi.org/10.1021/acs.energyfuels.2c00610.
[16] Yang S, Qiao H, Cheng B, Hu Q. Solvent extraction efficiency of an Eocene-aged organic-rich lacustrine shale. Mar Pet Geol 2021;126:104941. https://doi.org/10.1016/j.marpetgeo.2021.104941.
[17] Li J, Jiang C, Wang M, Xu L, Li M, Yu C, et al. Determination of in situ hydrocarbon contents in shale oil plays. Part 1: Is routine Rock–Eval analysis reliable for quantifying the hydrocarbon contents of preserved shale cores? Org Geochem 2022;170:104449. Doi: 10.1016/j.orggeochem.2022.104449.
[18] Li J, Wang M, Fei J, Xu L, Shao H, Li M, et al. Determination of in situ hydrocarbon contents in shale oil plays. Part 2: Two-dimensional nuclear magnetic resonance (2D NMR) as a potential approach to characterize preserved cores. Mar Pet Geol 2022;145. https://doi.org/10.1016/j.marpetgeo.2022.105890.
[19] Romero-Sarmiento MF. A quick analytical approach to estimate both free versus sorbed hydrocarbon contents in liquid-rich source rocks. Am Assoc Pet Geol Bull 2019;103:2031–43. https://doi.org/10.1306/02151918152.
[20] Mosher K, He J, Liu Y, Rupp E, Wilcox J. Molecular simulation of methane adsorption in micro- and mesoporous carbons with applications to coal and gas shale systems. Int J Coal Geol 2013;109–110:36–44. https://doi.org/10.1016/j.coal.2013.01.001.
[21] Falk K, Pellenq R, Ulm FJ, Coasne B. Effect of chain length and pore accessibility on alkane adsorption in kerogen. Energy Fuel 2015;29:7889–96. https://doi.org/10.1021/acs.energyfuels.5b02015.
[22] Luo Y, Xiao H, Liu X, Zheng T. Occurrence characteristics and influential factors of movable oil in nano-pores by molecular dynamics simulation. Colloids Surfaces A Physicochem Eng Asp 2022;655:130320. https://doi.org/10.1016/j.colsurfa.2022.130320.
[23] Xu Y, Lun Z, Pan Z, Wang H, Zhou X, Zhao C, et al. Occurrence space and state of shale oil: a review. J Pet Sci Eng 2022;211. https://doi.org/10.1016/j.petrol.2022.110183.
[24] Wang E, Feng Y, Guo T, Li M. Oil content and resource quality evaluation methods for lacustrine shale: a review and a novel three-dimensional quality evaluation model. Earth-Science Rev 2022;232:104134. https://doi.org/10.1016/j.earscirev.2022.104134.
[25] Zhang H, Huang H, Li Z, Liu M. Oil physical status in lacustrine shale reservoirs – a case study on eocene shahejie formation shales, Dongying Depression. East China Fuel 2019;257:116027. https://doi.org/10.1016/j.fuel.2019.116027.
[26] Slatt RM, O'Brien NR. Pore types in the Barnett and Woodford gas shales: contribution to understanding gas storage and migration pathways in fine-grained rocks. Am Assoc Pet Geol Bull 2011;95:2017–30. https://doi.org/10.1306/03301110145.
[27] Dong X, Xu W, Liu R, Chen Z, Lu N, Guo W. Insights into adsorption and diffusion behavior of shale oil in slit nanopores: A molecular dynamics simulation study. J Mol Liq 2022;359:119322. https://doi.org/10.1016/j.molliq.2022.119322.
[28] Ma C, Zhao X, Yang T, Jiang W, Guo B, Han G, et al. Mineralogy, organic geochemistry, and microstructural characterization of lacustrine Shahejie Formation, Qikou Sag, Bohai Bay Basin: contribution to understanding microcosmic storage mechanism of shale oil. J Pet Sci Eng 2022;209:109843. https://doi.org/10.1016/j.petrol.2021.109843.
[29] Jijun L, Weiming W, Qun C, Yinglin S, Xintong Y, Shansi T. Impact of hydrocarbon expulsion efficiency of continental shale upon shale oil accumulations in eastern China. Mar Pet Geol 2015;59:467–79. https://doi.org/10.1016/j.marpetgeo.2014.10.002.
[30] Su S, Jiang Z, Xuanlong S, Zhang C, Zou Q, Li Z, et al. The effects of shale pore structure and mineral components on shale oil accumulation in the Zhanhua Sag, Jiyang Depression, Bohai Bay Basin, China. J Pet Sci Eng 2018;165:365–74. https://doi.org/10.1016/j.petrol.2018.02.030.
[31] Zhong J, Wang P, Zhang Y, Yan Y, Hu S, Zhang J. Adsorption mechanism of oil components on water-wet mineral surface: a molecular dynamics simulation study. Energy 2013;59:295–300. https://doi.org/10.1016/j.energy.2013.07.016.
[32] Zhang Y, Fang T, Ding B, Wang W, Yan Y, Li Z, et al. Migration of oil/methane mixture in shale inorganic nano-pore throat: A molecular dynamics simulation study. J Pet Sci Eng 2020;187:106784. https://doi.org/10.1016/j.petrol.2019.106784.
[33] Han Y, Mahlstedt N, Horsfield B. The Barnett Shale: Compositional fractionation associated with intraformational petroleum migration, retention, and expulsion. Am Assoc Pet Geol Bull 2015;99:2173–201. https://doi.org/10.1306/06231514113.
[34] Jarvie DM. Components and processes affecting producibility and commerciality of shale resource systems. Geol Acta 2014;12:307–25. https://doi.org/10.1344/GeologicaActa2014.12.4.3.
[35] Hemmati-Sarapardeh A, Khishvand M, Naseri A, Mohammadi AH. Toward reservoir oil viscosity correlation. Chem Eng Sci 2013;90:53–68. https://doi.org/10.1016/j.ces.2012.12.009.
[36] Hou L, Ma W, Luo X, Liu J, Liu S, Zhao Z. Hydrocarbon generation-retention-expulsion mechanism and shale oil producibility of the permian lucaogou shale in the Junggar Basin as simulated by semi-open pyrolysis experiments. Mar Pet Geol 2021;125:104880. https://doi.org/10.1016/j.marpetgeo.2020.104880.
[37] Bagri A, Grantab R, Medhekar NV, Shenoy VB. Stability and formation mechanisms of carbonyl- and hydroxyl-decorated holes in graphene oxide. J Phys Chem C 2010;114:12053–61. https://doi.org/10.1021/jp908801c.
[38] Liang C, Wu J, Cao Y, Liu K, Khan D. Storage space development and hydrocarbon occurrence model controlled by lithofacies in the Eocene Jiyang Sub-basin, East China: Significance for shale oil reservoir formation. J Pet Sci Eng 2022;215:110631. https://doi.org/10.1016/j.petrol.2022.110631.
[39] Castro MA, Clarke SM, Inaba A, Arnold T, Thomas RK. Competitive adsorption of simple linear alkane mixtures onto graphite. J Phys Chem B 1998;102:10528–34. https://doi.org/10.1021/jp982965z.
[40] Zou C, Yang Z, Cui J, Zhu R, Hou L, Tao S, et al. Formation mechanism, geological characteristics and development strategy of nonmarine shale oil in China. Pet Explor Dev 2013;40:15–27. https://doi.org/10.1016/S1876-3804(13)60002-6.
[41] Zhao X, Zhou L, Pu X, Jin F, Han W, Shi Z, et al. Theories, technologies and practices of lacustrine shale oil exploration and development: a case study of Paleogene Kongdian Formation in Cangdong sag, Bohai Bay Basin. China Pet Explor Dev 2022;49:707–18. https://doi.org/10.1016/S1876-3804(22)60059-4.
[42] Song M, Liu H, Wang Y, Liu Y. Enrichment rules and exploration practices of Paleogene shale oil in Jiyang Depression, Bohai Bay Basin. China Pet Explor Dev 2020;47:242–53. https://doi.org/10.1016/S1876-3804(20)60043-X.
[43] Zhao W, Hu S, Guo X, Li J, Cao Z. New concepts for deepening hydrocarbon exploration and their application effects in the Junggar Basin. NW China Pet Explor Dev 2019;46:856–65. https://doi.org/10.1016/S1876-3804(19)60245-4.
[44] Xi K, Li K, Cao Y, Lin M, Niu X, Zhu R, et al. Laminae combination and shale oil enrichment patterns of Chang 73 sub-member organic-rich shales in the Triassic Yanchang Formation, Ordos Basin. NW China Pet Explor Dev 2020;47:1342–53. https://doi.org/10.1016/S1876-3804(20)60142-8.
[45] Shen Y, Jin Z, Su J, Li Z, Niu J. Characteristics of horizontal and vertical permeability of continental shale oil reservoirs in China: a case from Jiyang Depression in Bohai Bay Basin and Qianjiang Sag in Jianghan Baisn. Oil Gas Geol 2022;43:378–89. https://doi.org/10.11743/ogg20220211.
[46] Shi J, Jin Z, Liu Q, Zhang T, Fan T, Gao Z. Laminar characteristics of lacustrine organic-rich shales and their significance for shale reservoir formation: a case study of the Paleogene shales in the Dongying Sag, Bohai Bay Basin. China J Asian Earth Sci 2022;223:104976. https://doi.org/10.1016/j.jseaes.2021.104976.
[47] Guo S, Mao W. Division of diagenesis and pore evolution of a Permian Shanxi shale in the Ordos Basin. China J Pet Sci Eng 2019;182:106351. https://doi.org/10.1016/j.petrol.2019.106351.
[48] Hucheng D, Meiyan F, Wen Z, Liying Z, Xinhui X, Yilin L, et al. The pores evolution of lacustrine shale induced by smectite-to-illite conversion and hydrocarbon generation: upper Triassic Yanchang Formation, Ordos Basin. China J Pet Sci Eng 2021;202:108460. https://doi.org/10.1016/j.petrol.2021.108460.
[49] Xu S, Gou Q. The importance of laminae for China lacustrine shale oil enrichment: a review. Energies 2023;16. https://doi.org/10.3390/en16041661.
[50] Zhang M, Dai S, Pan S, Jing Z, Wu Z, Chen Y, et al. Deciphering the laminated botryococcus-dominated shales in saline lacustrine basin, Western Qaidam Basin, NW China: Implications for shale oil potential. Mar Pet Geol 2023;155:106397. https://doi.org/10.1016/j.marpetgeo.2023.106397.
[51] Liu B, Jin L, Hu C. Fractal characterization of silty beds/laminae and its implications for the prediction of shale oil reservoirs in Qingshankou formation of northern Songliao basin. NORTHEAST China Fractals 2019;27:1–12. https://doi.org/10.1142/S0218348X19400097.
[52] Lei Y, Luo X, Wang X, Zhang L, Jiang C, Yang W, et al. Characteristics of silty laminae in Zhangjiatan shale of southeastern Ordos Basin, China: Implications for shale gas formation. Am Assoc Pet Geol Bull 2015;99:661–87. https://doi.org/10.1306/09301414059.
[53] Guo X, Zhou L, Pan Y, Huang Z, Chen X, Mu S, et al. Pore structure and oil-bearing property of laminated and massive shale of Lucaogou Formation in Malang Sag. Santanghu Basin Geol J 2024;59:980–99. https://doi.org/10.1002/gj.4904.
[54] Luo L, Qi J, Li H, Dong Y, Zhang S, Zhang X, et al. Geometry and Evolution of the Cangdong Sag in the Bohai Bay Basin, China: Implications for Subduction of the Pacific Plate. Sci Rep 2017;7:2–8. https://doi.org/10.1038/s41598-017-15759-x.
[55] Yang T, Cao Y, Wang Y, Cai L, Liu H, Jin J. Sedimentary characteristics and depositional model of hyperpycnites in the gentle slope of a lacustrine rift basin: a case study from the third member of the Eocene Shahejie Formation, Bonan Sag, Bohai Bay Basin. Eastern China Basin Res 2023;35:1590–618. https://doi.org/10.1111/bre.12766.
[56] Feng B, He Y, Li H, Li T, Du X, Huang X, et al. Paleogeographic reconstruction of an ancient source-to-sink system in a lacustrine basin from the Paleogene Shahejie formation in the Miaoxibei area (Bohai Bay basin, east China). Front Earth Sci 2023;11:1–19. https://doi.org/10.3389/feart.2023.1247723.
[57] Song Y, Ye X, Shi Q, Huang C, Cao Q, Zhu K, et al. A comparative study of organic-rich shale from turbidite and lake facies in the Paleogene Qikou Sag (Bohai Bay Basin, East China): Organic matter accumulation, hydrocarbon potential and reservoir characterization. Palaeogeogr Palaeoclimatol Palaeoecol 2022:594. https://doi.org/10.1016/j.palaeo.2022.110939.
[58] Huang C, Wang H, Wu Y, Wang J, Chen S, Ren P, et al. Genetic types and sequence stratigraphy models of Palaeogene slope break belts in Qikou Sag, Huanghua Depression, Bohai Bay Basin. Eastern China Sediment Geol 2012;261–262:65–75. https://doi.org/10.1016/j.sedgeo.2012.03.005.
[59] Wu Z, Zhao X, Wang E, Pu X, Lash G, Han W, et al. Sedimentary environment and organic enrichment mechanisms of lacustrine shale: a case study of the Paleogene

Shahejie Formation, Qikou Sag. Bohai Bay Basin Palaeogeogr Palaeoclimatol Palaeoecol 2021;573:110404. https://doi.org/10.1016/j.palaeo.2021.110404.
[60] Pu X, Zhou L, Xiao D, Hua S, Chen C, Yuan X, et al. Lacustrine carbonates in the southwest margin of the Qikou Sag, Huanghua Depression. Bohai Bay Basin Pet Explor Dev 2011;38:136–44. https://doi.org/10.1016/S1876-3804(11)60022-0.
[61] Pu X, Han W, Hua S, Zhang W, Chen C. Main controlling factors and dominant reservoir series analysis of Es 3 in the Qibei area of Qikou sag. Acta Geol Sin (English Ed 2013;87:219–31. https://doi.org/10.1111/1755-6724.12043.
[62] Khan D, Liang C, Qiu L, Kamran MIRZA, Wang Y, Kashif M, et al. Depositional environment and lithofacies analyses of eocene lacustrine shale in the Bohai Bay Basin: insights from mineralogy and elemental geochemistry. Acta Geol Sin (English Ed 2023;97:589–609. https://doi.org/10.1111/1755-6724.14985.
[63] Schlanser K, Grana D, Campbell-Stone E. Lithofacies classification in the Marcellus Shale by applying a statistical clustering algorithm to petrophysical and elastic well logs. Interpret (United Kingdom) 2016;4:SE31–49. https://doi.org/10.1190/INT-2015-0128.1.
[64] White RJ, Budarin V, Luque R, Clark JH, Macquarrie DJ. Tuneable porous carbonaceous materials from renewable resources. Chem Soc Rev 2009;38:3401–18. https://doi.org/10.1039/b822668g.
[65] Alothman ZA. A review: fundamental aspects of silicate mesoporous materials. Materials (Basel) 2012;5:2874–902. https://doi.org/10.3390/ma5122874.
[66] Fleury M, Gimmi T, Mazurek M. Porewater content, pore structure and water mobility in clays and shales from NMR Methods. Clays Clay Miner 2022;70:417–37. https://doi.org/10.1007/s42860-022-00195-4.
[67] Wan T, Zhang J, Wu B. NMR and CT characterizing the influence of O2 in air injection performance in shale oil cores. Fuel 2024;356:129639. https://doi.org/10.1016/j.fuel.2023.129639.
[68] Zhang C, Jiang F, Hu T, Chen D, Huang L, Jiang Z, et al. Oil occurrence state and quantity in alkaline lacustrine shale using a high-frequency NMR technique. Mar Pet Geol 2023;154:106302. https://doi.org/10.1016/j.marpetgeo.2023.106302.
[69] Gou Q, Xu S, Chen Z, Wu Z. Novel method for the classification of shale Oil reservoirs associated with mobility: inspiration from gas adsorption and multiple isothermal stage pyrolysis. Energy Fuel 2023;37:9121–30. https://doi.org/10.1021/acs.energyfuels.3c01172.
[70] Zhang H, Huang H, Li Z, Liu M. Comparative study between sequential solvent-extraction and multiple isothermal stages pyrolysis: A case study on Eocene Shahejie Formation shales, Dongying Depression. East China Fuel 2020;263:116591. https://doi.org/10.1016/j.fuel.2019.116591.
[71] Gai H, Xiao X, Cheng P, Tian H, Fu J. Gas generation of shale organic matter with different contents of residual oil based on a pyrolysis experiment. Org Geochem 2015;78:69–78. https://doi.org/10.1016/j.orggeochem.2014.11.001.
[72] Li J, Jiang C, Wang M, Xu L, Li M, Yu C, et al. Determination of in situ hydrocarbon contents in shale oil plays. Part 1: Is routine Rock-Eval analysis reliable for quantifying the hydrocarbon contents of preserved shale cores? Org Geochem 2022;170:104449. https://doi.org/10.1016/j.orggeochem.2022.104449.